Visible Blind Quadrant Sun Position Sensor in a Silicon Carbide Technology

Romijn, Joost; Vollebregt, Sten; May, Alexander ; Erlbacher , Tobias ; van Zeijl, Henk W.; Leijtens, Johan; Zhang, Guoqi; Sarro, Pasqualina M.

DOI
10.1109/MEMS51670.2022.9699533

Publication date
2022

Document Version
Final published version

Published in
Proceedings of the 2022 IEEE 35th International Conference on Micro Electro Mechanical Systems Conference (MEMS)

VISIBLE BLIND QUADRANT SUN POSITION SENSOR IN A SILICON CARBIDE TECHNOLOGY

Joost Romijn[1], Sten Vollebregt[1], Alexander May[2], Tobias Erlbacher[2], Henk W. van Zeijl[1], Johan Leijtens[3], Guoqi Zhang[1], and Pasqualina M. Sarro[1]

[1]Laboratory of Electronic Components, Technology and Materials (ECTM), Department of Microelectronics, Delft University of Technology, THE NETHERLANDS, [2]Fraunhofer Institute for Integrated Systems and Devices Technology IISB, GERMANY, and [3]Lens R&D BV, Noordwijk, THE NETHERLANDS

2022 IEEE 35th International Conference on Micro Electro Mechanical Systems Conference (MEMS) | 978-1-6654-0911-7/22/$31.00 ©2022 IEEE | DOI: 10.1109/MEMS51670.2022.9699533

ABSTRACT

In this paper, we present a quadrant sun position sensor microsystem device in a silicon carbide technology that operates in a field-of-view of ±33° and reaches a mean error of 1.9° in this range. This will allow, for the first time, an inherently visible blind sun position sensor in a CMOS compatible technology. Opto-electronic integration of the photodetectors and CMOS readout circuitry on-chip is vital to compete with the performance of silicon state-of-the-art and for the concept to be adopted by industry, which is where previous implementations of visible blind sun sensors are lacking.

KEYWORDS

4H-SiC; silicon carbide; sun position sensors; UV photodetectors; wide bandgap semiconductors

INTRODUCTION

The sun position sensor is an attitude sensor that is able to provide information on the direction towards the Sun. It is a vital device for satellite attitude control in outer space and is continuously subjected to further improvements. Silicon state-of-the-art commercial sun position sensors suffer from an inherent sensitivity to the albedo, which is the visible light reflected by the Earth. This undesired sensitivity is directly related the semiconductor bandgap, as this determines the photodetector spectral response. The importance of visible blindness for sun position sensors was previously recognized and implemented in an InGaAs technology [1] and a GaN-on-sapphire technology [2] to target spectral bands in IR and UV respectively. Both of the previous implementations, as well as this work, rely on the collimating sun sensor architecture [3].

Wide bandgap materials such as gallium nitride (GaN) and silicon carbide (SiC) have been extensively researched for UV photodetection over the past decades. The future market of wide bandgap materials is expected to grow in the next decade [4], which we know from silicon technology brings device cost reduction and further improvements. This opens the door to inherently visible blind sun position sensor devices by implementation in wide bandgap materials. For on-chip readout electronics, SiC is at present considered the most mature technology and best known are the CMOS HiTSiC [5-6] and BJT HOTSiC [7-8] technologies, developed by Raytheon Systems Limited and the KTH university respectively. Unfortunately, the HiTSiC technology was discontinued in 2018, which left the need for a new and open SiC CMOS technology. This need is addressed by the recent development of the SiC CMOS at Fraunhofer IISB [9-11].

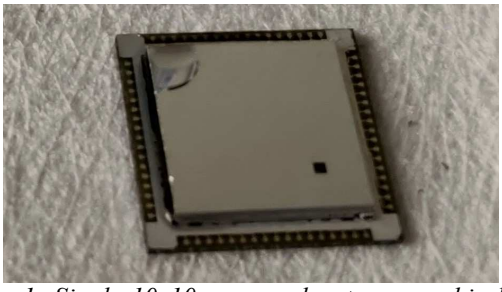

Figure 1: Single 10x10 mm quadrant sensor chip before packaging with cyanoacrylate glue on the top left. Note that this is a multi-project chip and the actual sensor is located at the bottom right under the opening in the metal mask.

This work reports on a quadrant sun position sensor in 4H-SiC (Figure 1), which builds on the previously reported integrated 3D optics approach [12] to aim for miniaturization of the device in the future. In contrast to previous work, the sensing element is implemented in silicon carbide rather than silicon, in favor of a high UV-to-VIS selectivity ratio. Silicon carbide also has a higher radiation hardness, which in turn reduces the packaging demand. This opens the possibility for an inherently visible blind sun position sensor technology. Moreover, the silicon carbide technology that is used allows for the integration of on-chip readout electronics, which has been previously lacking in other technologies.

EXPERIMENTAL

Quadrant Sensor Architecture

The schematic overviews of a quadrant sun position sensor in Figure 2 show four quadrant photodetectors on the substrate and a light mask that casts a light spot on the detectors. The distance between the detectors and light mask is implemented by a highly transparent sapphire optical window added during device packaging. The angles $\angle\theta$ and $\angle\varphi$ provide the cartesian direction vector to the light source, which are extracted from the detectors response. In the plane of the four photodetectors, these angles correspond to a lateral displacement of the light spot in x and y direction through

$$\angle\theta = \tan^{-1}\left(\frac{\Delta x}{h}\right) \quad \text{and} \quad \angle\varphi = \tan^{-1}\left(\frac{\Delta y}{h}\right), \tag{1}$$

where h corresponds to the thickness of the optical window. The determination of Δx and Δy is done through a readout scheme that compares the illuminated areas of the four photodetectors. Snell's Law is employed to account for refraction of the angles into the optical window.

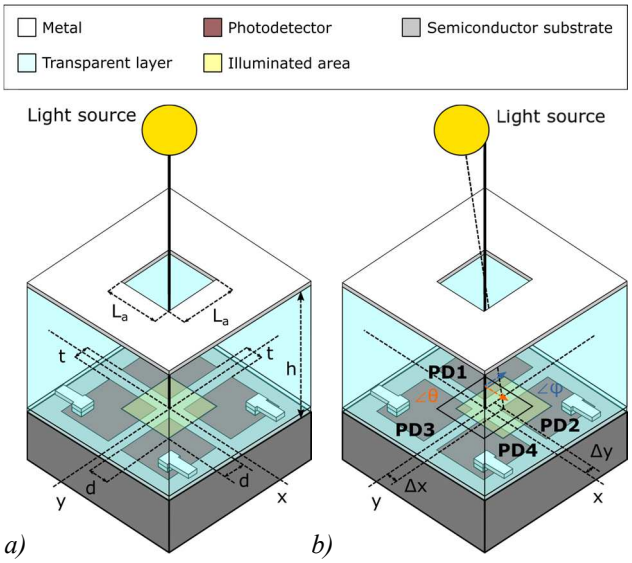

Figure 2: Schematic overview of the quadrant sun position sensor for a) perpendicular illumination and b) arbitrary direction. The direction towards the light source is defined by ∠θ (orange) and ∠φ (blue) and the corresponding lateral displacement of the light spot is described by Δx and Δy. Including t as the distance between photodetectors and the light spot overlap is d at perpendicular illumination.

Device Fabrication

The photodetectors are implemented in the novel open silicon carbide CMOS technology [9-11] developed by Fraunhofer IISB in Germany. The fabrication process front-end-of-line (FEOL) is implemented by ion implantation, which is used for the photodetector realization. The back-end-of-line (BEOL) employs a sophisticated silicidation step to implement the metal contacts to the doped layers. By implementing the visible blind sun position sensor in this silicon carbide technology, future implementations can integrate CMOS readout circuitry on-chip to achieve high performance sensors that can outperform the state-of-the-art in industry. Furthermore, such opto-electronic integration enables other detector architectures, like a scalable array of active pixels [13], and even additional functionalities such as temperature sensing [14-15].

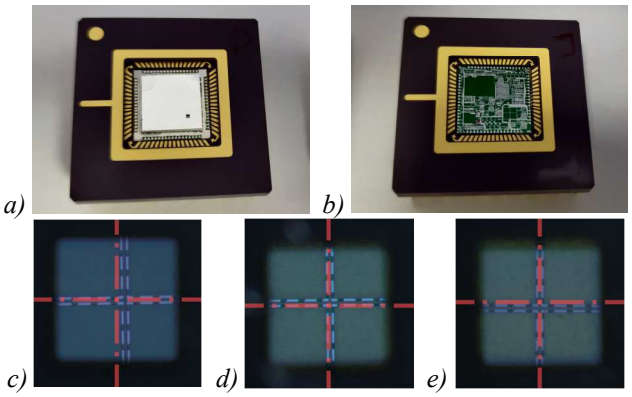

Figure 3:Photograph of the a) packaged quadrant sun position sensor device and b) packaged bare silicon carbide multi-project chip. The alignment of the center of the quadrant sensor and pinhole is optically verified for c) device 1, d) device 2 and e) device 3 with ideal case in red.

The collimating sun position sensor is implemented by alignment of a sapphire optical window to the silicon carbide device on chip level. Sapphire has a refraction index of 1.8 in the target spectral range. It is secured in place using cyanoacrylate glue at one corner to avoid interference with the optical sensor. The optical window is pre-coated by a 2 µm aluminium layer by sputter deposition and includes a 500x500 µm square opening. Three sensors are packaged and verified for overlay alignment (Figure 3).

RESULTS AND DISCUSSION

Photodetector Response

The electrical response of the bare 0.81 cm^2 photodetectors used in the quadrant sensor is investigated for different illumination conditions (Figure 4). The photo-to-dark current ratio (PDCR) towards ambient light (enclosure open) and UV light equal 0.998 and 157 respectively, from which excellent preliminary visible blindness is concluded. The considered UV light source is a single 5 mW SMD3535 265 nm UV-C LED at a distance of 4-5 cm. For partial illumination of the photodetectors in the quadrant sensor, the generated photocurrent equals

$$I_{PD}(\theta,\varphi) = I_0(\theta,\varphi)\frac{A_i(\theta,\varphi)}{A_{tot}}, \quad (2)$$

where I_0 is the photocurrent that is generated at full area illumination at the specific angles, A_i the illuminated photodetector area and A_{tot} the total photodetector area.

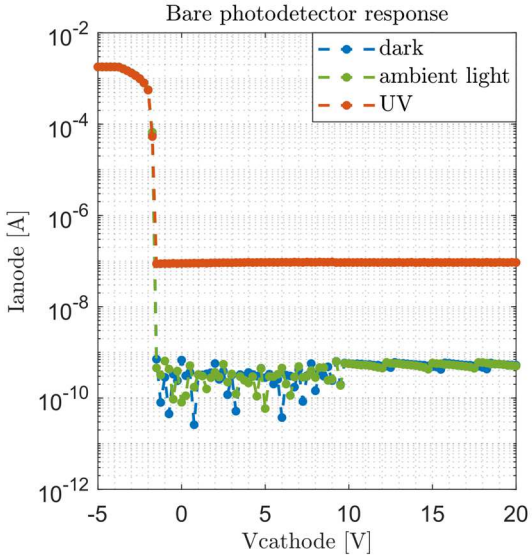

Figure 4: Electrical response of a bare photodetector (Figure 3b) to different illumination conditions.

Readout Methodology

The first step in the determination of the direction vector towards the light source, is to identify which of the four photodetectors is generating the most current. This photodetector is identified as the reference and linked to this are the photodetectors PD_x and PD_y to be used for determining Δx and Δy as listed in Table 1. Then, the respective generated photocurrents for the identified Δx and Δy photodetectors are divided by that of the reference photodetector, which results in

$$R_x(\theta) = \frac{I_{PD,x}(\theta,\varphi)}{I_{PD,r}(\theta,\varphi)} \quad \text{and} \quad R_y(\varphi) = \frac{I_{PD,y}(\theta,\varphi)}{I_{PD,r}(\theta,\varphi)}. \tag{3}$$

At this point it cannot yet be concluded that these ratios are solely dependent on a single angle in the direction vector. To reveal this, the areas A of the specific photodetector functions are first reduced to multiplications

$$\begin{aligned} A_r(\theta,\varphi) &= \big(d + \Delta x(\theta)\big)\big(d + \Delta y(\varphi)\big) \quad \text{and} \\ A_x(\theta,\varphi) &= \big(d - \Delta x(\theta)\big)\big(d + \Delta y(\varphi)\big) \quad \text{and} \\ A_r(\theta,\varphi) &= \big(d + \Delta x(\theta)\big)\big(d - \Delta y(\varphi)\big). \end{aligned} \tag{4}$$

These area definitions are substituted in Equation 2 for each photodetector, which in turn is substituted in Equation 3 to obtain

$$R_x(\theta) = C_x \frac{d-\Delta x(\theta)}{d+\Delta x(\theta)} \quad \text{and} \quad R_y(\varphi) = C_y \frac{d-\Delta y(\varphi)}{d+\Delta y(\varphi)}. \tag{5}$$

Note that the maximum generated current should be identical for each photodetector. However, to account for any mismatch, constants C_x and C_y are considered which are ideally equal to 1. These relations show that each respective ratio of measured photocurrents is indeed dependent on only Δx or Δy. As such, rewriting these relations to solve the lateral displacements yields

$$\Delta x(\theta) = d\frac{C_x - R_x(\theta)}{C_x + R_x(\theta)} \quad \text{and} \quad \Delta y(\varphi) = d\frac{C_y - R_y(\varphi)}{C_y + R_y(\varphi)}. \tag{6}$$

Finally, the dimension d is estimated by assuming that the light spot is of equal dimension as the light mask. Which is true by assuming parallel incident rays and no other optical effects in the optics. This thus results in

$$d \approx \frac{L_a - t}{2}. \tag{7}$$

Table 1: Function definition of the photodetectors from Figure 2, identifying the reference by the photodetector that generates the maximum photocurrent.

Reference	PDx	PDy
PD1	PD2	PD3
PD2	PD1	PD4
PD3	PD4	PD1
PD4	PD3	PD2

Angular Response

The optical measurement setup (Figure 5) allows for rotation of the interface PCB over a single axis, while the UV LED point source is at a fixed spot. To measure two perpendicular rotation axis ($\angle\theta$ and $\angle\varphi$), the PCB orientation is rotated in the clamp. The bias of all four photodetectors is varied for each angle composition to investigate the optimal bias value, with peak operation at 12.5 V. The resulting angular responses (Figure 6) are calculated using Equations 6 and 1 and indicate definite angular sensitivity in a field-of-view of ±33°, that comply with the ideal curve with a mean error of 2.9° for the best functioning sensor in the dataset (Table 2). This is further improved to a mean error of 1.9° by numerical calculation of calibration constants C_x and C_y.

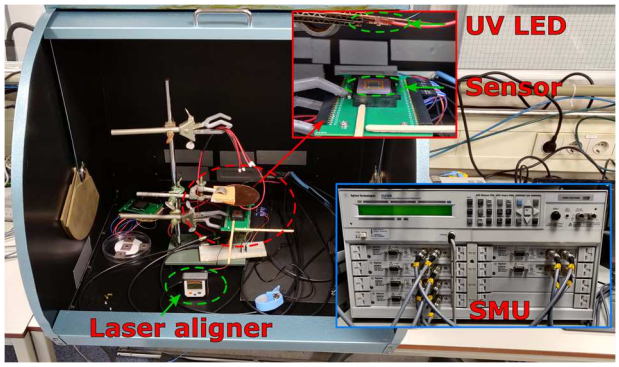

Figure 5: Angular response measurement setup. A 5 mW SMD3535 265 nm UV-C LED is mounted on a copper plate perpendicular to the sensor and spaced 4-5 cm from the sensor. The PCB is rotated over one axis and aligned using a Laserligner DigiLevel Plus. The system maximum alignment error is estimated at 2°. The sensor outputs are measured by Agilent E5287A source-measurement units.

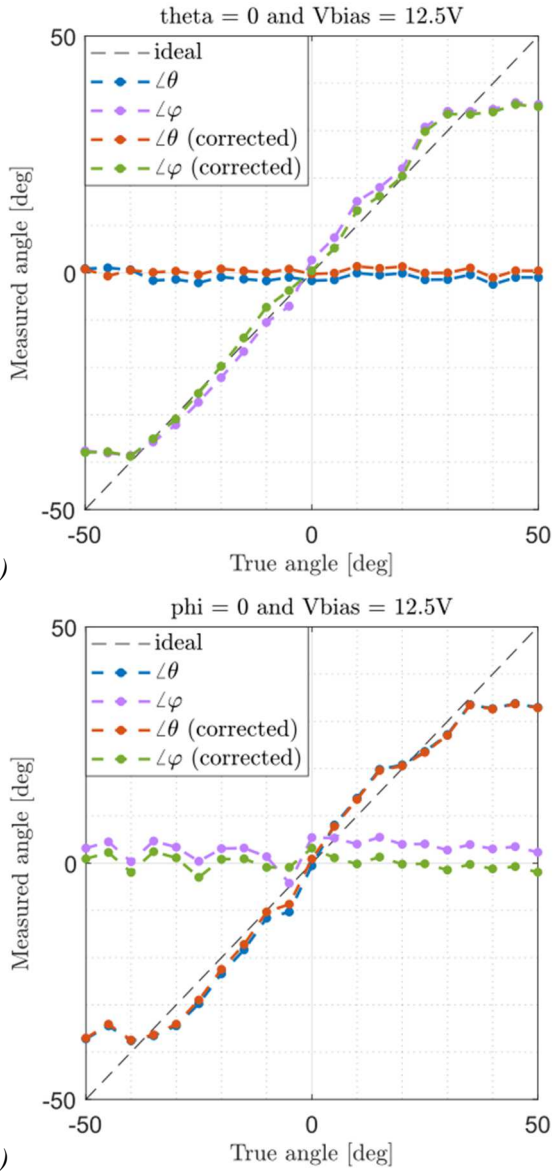

Figure 6: Raw and corrected angular response of device 3, when a) $\angle\theta$ is constant while sweeping $\angle\varphi$ and b) vice versa. The substrate and each photodetector are biased at 0V and 12.5V respectively.

Table 2: Raw and corrected mean error in the field-of-view of three identical devices. The correction factors C_x and C_y are numerically calculated and are unique for each device. Note that the calibration factors are vectors of length 4, as each of the four cases in Table 1 has a unique combination of C_x and C_y.

Device	Error (raw)	Error (corrected)
1	4.3°	2.8°
2	2.9°	1.9°
3	3.1°	2.6°

CONCLUSIONS

A collimating quadrant sun position sensor with excellent inherent visible blindness was demonstrated. The 0.81 cm^2 photodetector sensing elements are implemented in a 4H-SiC technology, to target the UV spectral range. Additionally, a pre-coated sapphire optical window with high transmittance in UV light is used for overlaying the light mask at a distance to the photodetectors at chip-level. The best performing device had a mean error of 1.9° over a ±33° field-of-view.

Future work benefits from the potential of on-chip CMOS readout electronics in the Fraunhofer IISB technology. This also allows for integration of other reported sensors in the same technology. The next generation should include wafer-level integration of the optical windows with aligned light mask to ensure a scalable and reproducible technology. This can be realized by exploiting existing wafer-level packaging techniques.

ACKNOWLEDGEMENTS

The authors thank the Delft University of Technology Else Kooi Laboratory staff and the Fraunhofer IISB laboratory staff for processing support. Furthermore the authors thank the Dutch Technology Foundation (STW), which is part of The Netherlands Organization for Scientific Research (NWO), and which is partly funded by the Ministry of Economic Affairs, for financially supporting this work under project number 16247.

REFERENCES

[1] H. W. Wu, A. Emadi, G. de Graaf, J. Leijtens and R. F. Wolffenbuttel, “Design and fabrication of an albedo insensitive analog sun sensor”, in *Procedia Engineering*, vol. 25, pp. 527-530, 2011.

[2] R. A. Miller, H. So, H. C. Chiamori, A. J. Suria, C. A. Chapin and D. G. Senesky, “A microfabricated sun sensor using GaN-on-sapphire ultraviolet photodetector arrays”, in *Review on Scientific Instruments*, vol. 97, 095003, 2016.

[3] L. S. Salgado-Conrado, “A review on sun position sensors used in solar applications”, in *Renewable and Sustainable Energy Reviews*, vol. 82, pp. 2128-2146, 2018.

[4] IEEE Power Electronics Society (PELS), “International Technology Roadmap for Wide Bandgap Power Semiconductors (ITRW)”, 2019.

[5] R. A. R. Young, D. T. Clark, J. D. Cormack, A. E. Murphy, D. A. Smith, R. F. Thompson, E. P. Ramsay and S. Finney, “High temperature digital and analogue integrated circuits in silicon carbide”, in *Materials Science Forum*, vol. 740-742, pp. 1065-1068, 2013.

[6] E. P. Ramsay, J. Breeze, D. T. Clark, A. E. Murphy, D. A. Smith, R. F. Thompson, S. Wright, R. A. R. Young and A. Horsfall, “High temperature CMOS circuits on silicon carbide”, in *Materials Science Forum*, vol. 821-823, pp. 859-862, 2015.

[7] L. Lanni, B. G. Malm, M. Östling and C.-M. Zetterling, “Lateral p-n-p transistors and complementary SiC bipolar technology”, in *IEEE Electron Device Letters*, vol. 35, pp. 428-430, 2014.

[8] C.-M. Zetterling, A. Hallén, R. H. S. Kargarrazi, L. Lanni, B. G. Malm, S. Mardani, H. Norström, A. Rusu, S. S. Suvanam, Y. Tian and M. Östling, “Bipolar integrated circuits in SiC for extreme environment operation”, in *Semiconductor Science and Technology*, vol. 32, 034002, 2017.

[9] J. Romijn, S. Vollebregt, L. M. Middelburg, B. El Mansouri, H. W. van Zeijl, A. May, T. Erlbacher, G. Q. Zhang and P. M Sarro, “Integrated digital and analog circuit blocks in a scalable silicon carbide CMOS technology”, in *IEEE Transactions on Electron Devices*, 2021.

[10] A. Abbasi, S. Roy, R. Murphree, A.-U. Rashid, M. M. Hossain, P. Lai, J. Fraley, T. Erlbacher, Z. Chen and A. Mantooth, “Characterization of a silicon carbide BCD process for 300 °C circuits”, in *IEEE 7th Workshop on Wide Bandgap Power Devices and Applications (WiPDA)*, pp. 231-236, 2019.

[11] M. Albrecht, T. Erlbacher, A. J. Bauer and L. Frey, “Improving 5V digital 4H-SiC CMOS ICs for operating at 400 °C using PMOS channel implantation”, in *Materials Science Forum*, vol. 963, pp. 827-831, 2019.

[12] J. Romijn, S. Vollebregt, H. W. van Zeijl, G. Q. Zhang, J. Leijtens and P. M. Sarro, “Towards a scalable sun position sensor with monolithic integration of the 3D optics for miniaturized satellite attitude control”, in *34th International Conference on Micro Electro Mechanical Systems (MEMS)*, pp. 642-645, 2021.

[13] N. Xie and A. J. P. Theuwissen, “Low-power high accuracy micro-digital sun sensor by means of a CMOS image sensor”, in *Journal of Electronic Imaging*, vol. 22, 033030, 2013.

[14] C. D. Matthus, L. Di Benedetto, M. Kocher, A. J. Bauer, G. D. Licciardo, A. Rubino and T. Erlbacher, “Feasibility of 4H-SiC p-i-n diode for sensitive temperature measurements between 20.5 K and 802 K”, in *IEEE Sensors Journal*, vol. 19, pp. 2871-2877, 2019.

[15] J. Romijn, L. M. Middelburg, S. Vollebregt, B. El Mansouri, H. W. van Zeijl, A. May, T. Erlbacher, G. Q. Zhang and P. M. Sarro, “Resistive and CTAT temperature sensors in a silicon carbide CMOS technology”, in *IEEE Sensors*, 2021.

CONTACT

*J. Romijn; e-mail: J.Romijn@tudelft.nl